Cement and Concrete Research 41 (2011) 955–963

Contents lists available at ScienceDirect

Cement and Concrete Research

journal homepage: http://ees.elsevier.com/CEMCON/default.asp

Influence of slag chemistry on the hydration of alkali-activated blast-furnace slag — Part I: Effect of MgO

M. Ben Haha, B. Lothenbach *, G. Le Saout, F. Winnefeld

Empa, Swiss Federal Laboratories for Materials Science and Technology, Laboratory for Concrete and Construction Chemistry, Ueberlandstrasse 129, 8600 Dübendorf, Switzerland

ARTICLE INFO

Article history:
Received 14 February 2011
Accepted 3 May 2011

Keywords:
Alkali activated slags D
MgO (D)
Hydration mechanisms A
Microstructure (B)
Mechanical strength C

ABSTRACT

The hydration and the microstructure of three alkali activated slags (AAS) with MgO contents between 8 and 13 wt.% are investigated. The slags were hydrated in the presence of two different alkaline activators, NaOH and $Na_2SiO_3 \cdot 5H_2O$ (WG). Higher MgO content of the slag resulted in a faster reaction and higher compressive strengths during the first days. The formation of C(−A)–S–H and of a hydrotalcite-like phase was observed in all samples by X-ray diffraction (XRD), thermal analysis (TGA) and scanning electron microscopy (SEM) techniques. Increasing the MgO content of the slag from 8 to 13% increased the amount of hydrotalcite and lowered the Al uptake by C–S–H resulting in 9% higher volume of the hydrates and a 50 to 80% increase of the compressive strength after 28 days and longer for WG activated slag pastes. For NaOH activated slags only a slight increase of the compressive strength was measured.

1. Introduction

Alkali-activated binders based on ground granulated blast-furnace slag represent a viable and sustainable alternative to Portland cement since they use by-products of other industrial manufacturing processes. If one ton of slag replaces one ton of clinker, about 800 kg of CO_2 emissions can be "saved" [1,2]. Thus, the use of slag has important economical and environmental implications. Although a large proportion of global slag is used by the building industry, there is still a proportion remaining which is not yet used due to insufficient reactivity. The easiness of activation and the hydration of the slags depend mainly upon the mineralogical composition and fineness of the slag and on the type of the alkaline activator used. The addition of alkalis stimulates the dissolution of the slag and thus the formation of hydration products, mainly calcium silicate hydrates incorporating significant amounts of aluminium (C(−A)–S–H), hydrotalcite-like phase and strätlingite [3–5]. Activated slag systems often exhibit a rapid strength development, and using the adequate activators can lead to rapid setting, good durability and high resistance to chemical attack [6–8].

Many aspects of the chemistry of slag hydration activated by alkali still need to be explored, impeding the solution of the remaining practical problems and obstructing a wider application of this kind of binder. Probably most studies on AAS are focussed on the activator and not on slag chemistry. Knowing that "good slags" (=easily activated in a cementitious environment) are already largely used, a better understanding of the effects of the chemical composition of the slag could indicate ways to use less reactive slags efficiently. Understanding the hydration and development of the microstructure is the key to understand the performance of slags. Questions regarding the influence of different components such as mineral additions or slag composition on the hydration process and mechanical strength are of great interest as they have a major impact on the applicability of any construction material. The present study aims to investigate the effect of the MgO content in the slag on the kinetics of slag reaction and on compressive strength.

Experimental studies on the effect of MgO on slags are rare. In the iron-making process, the slag–iron interfacial tension was found to slightly increase with increasing MgO content in the slag [9]. It was reported that the MgO content of slag has a beneficial effect on the soundness of the autoclaved Portland cement–slag blends if the MgO was bound in non reactive phases such as merwinite, but was harmful for autoclaved cements when MgO was present as more reactive periclase [10].

An investigation, where 30% Portland cement was blended with 5.4% of anhydrite plus gypsum and 65% of different granulated blastfurnace slags, observed that the highest compressive strength of the mortars was measured at high Al_2O_3 and low MgO/Al_2O_3, i.e. where a high quantity of ettringite formed and little hydrotalcite [11]. In alkali activated slag systems, it has been reported that a small amount of crystalline phases in the slags and/or more MgO increased the compressive strength, whilst the presence of more Al_2O_3 had a negative effect [12].

The present study aims to investigate the effect of MgO on the hydration properties of alkali activated slag over 1 year, using three slags with different MgO contents whilst the contents of the other oxides are nearly constant. Sodium silicate and sodium hydroxide are

* Corresponding author. Tel.: +41 44 823 47 88; fax: +41 44 823 40 35.
E-mail address: barbara.lothenbach@empa.ch (B. Lothenbach).

0008-8846/$ – see front matter © 2011 Elsevier Ltd. All rights reserved.
doi:10.1016/j.cemconres.2011.05.002

used as activators. A multi-method approach involving strength measurements, calorimetry, X-ray diffraction, thermogravimetry, scanning electron microscopy and thermodynamic modelling is used to study the hydration mechanisms.

2. Materials and methods

2.1. Slags

Three technical slags with different MgO contents of 7.7 wt.% (M8), 10.5 wt.% (M11) and 13.2 wt.% (M13) were used. The slags were ground in a laboratory ball mill to a specific surface of 5000 ± 100 cm^2/g (Table 1).

2.2. Binder formulations

Two alkaline activators, NaOH (3.77 g/100 g slag) and sodium water glass $Na_2SiO_3 \cdot 5H_2O$ (WG) (10.0 g/100 g slag) were used, resulting in the same Na_2O content in both cases. A water to binder ratio of 0.40 was applied.

2.3. Methods

2.3.1. Anhydrous slags

The chemical composition of the anhydrous slags was analysed by XRF using a Philips PW 2400 instrument. The particle size distribution was determined with a laser granulometer Malvern Mastersizer X. X-ray powder diffraction (XRD) was carried out with an incident beam monochromator and CuKα radiation (λ = 1.54 Å) on a PANalytical X'Pert Pro MPD diffractometer in θ–2θ configuration with an angular scan 5–65° 2θ and an X'Celerator detector. An internal standard (CaF_2) was added to the anhydrous slag in order to deduce the amorphous content of the material and to follow the position of the hump around 0.3 nm (~30° 2θ; Fig. 1) that characterises the amorphous slag [13,14]. The ^{29}Si NMR spectra were recorded on a Bruker ASX 400 spectrometer (9.39 T magnetic field) at 79.5 MHz and at 4.5 kHz spinning rate in 7 mm ZrO_2 rotor. The ^{29}Si chemical shift of the peaks was analysed using the Q^n classification, where the Si tetrahedron is connected to n Si tetrahedra with n varying from 0 to 4. The ^{29}Si chemical shift was referenced relative to tetramethylsilane $Si(CH_3)_4$ (TMS) at 0 ppm.

2.3.2. Hydration

To study hydration, pastes with water to binder ratio of 0.40 were prepared. The initial water content of WG was taken into account in order to have same water content for the hydration. The activators were dissolved prior to the mixing in the water to ensure a good repartition in the paste.

About 5 g of paste were filled in a glass vial, sealed and loaded into a TAM Air isothermal calorimeter in order to determine the rate of heat of hydration during the first week at 20 °C.

The compressive strengths were determined on duplicate paste cubes (25 × 25 × 25 mm) for each testing age. They were cured in sealed plastic vessels at 20 °C, demolded at each testing ages and cut into the required size. The compressive strength was also determined on duplicate mortar prisms (40 × 40 × 160 mm) for different testing age up to 28 days according to EN 196–1. The mortar was prepared with a water/binder ratio of 0.45, a binder/aggregate ratio of 1/3 using standardised aggregate according to EN 196-1 (<2.5 mm) and the same quantity of alkali activator as in the pastes. The samples were cured under saturated conditions at 20 °C.

For thermogravimetric analysis (TGA) and X-ray diffraction analysis (XRD), the hydration was stopped by solvent exchange with isopropanol. Prior to measurement the samples were ground below 63 μm. Samples of about 20 mg were weighed into aluminium oxide crucibles. TGA measurements were performed between 30 and 980 °C at a heat rate of 20 K/min in a Mettler Toledo TGA/SDTA851. The standard deviation on three independent measurements at different tested ages is not larger than 0.2 g/100 g for total bound water. XRD was performed as described above, but without CaF_2 standard.

For the microscopical investigations slices of hydrated samples were cut. They were immediately immersed in isopropanol and subsequently dried at 40 °C for 24 h. They were then impregnated using a low viscosity epoxy resin and polished down to ¼ μm. The samples were further coated with carbon and examined using a Philips ESEM FEG XL 30 scanning electron microscopy (SEM). Backscattered electron images (BSE) were analysed quantitatively to determine the capillary porosity and the degree of reaction at

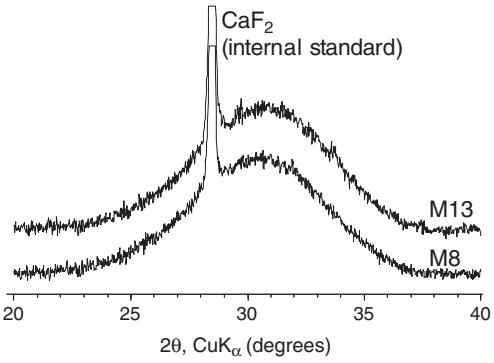

Fig. 1. XRD patterns of the M8 and M13 slags.

Table 1
Chemical composition and granular properties of the slags used in the study.

	M8	M11	M13
Loi	−0.8	−0.86	−0.4
SiO_2	38.2	37.1	36.4
Al_2O_3	12.0	11.5	11.3
Fe_2O_3	1.6	1.8	1.4
CaO	35.8	34.6	33.4
MgO	7.7	10.5	13.2
SO_3	1.4	1.2	0.36
K_2O	1.2	1.1	1.0
Na_2O	0.41	0.40	0.52
TiO_2	0.50	0.48	0.47
Mn_2O_3	1.5	1.5	1.4
P_2O_5	0.03	0.03	0.02
Ca/Si molar	1.00	1.00	0.98
Mg/Al molar	0.81	1.16	1.48
Density (g/cm^3)	2.92	2.93	2.94
Blaine (g/cm^2)	4990	5070	5010
% R90 μm	0	0	0
% R18 μm	23.0	18.7	21.8
% R 3 μm	76.9	74.7	76.9

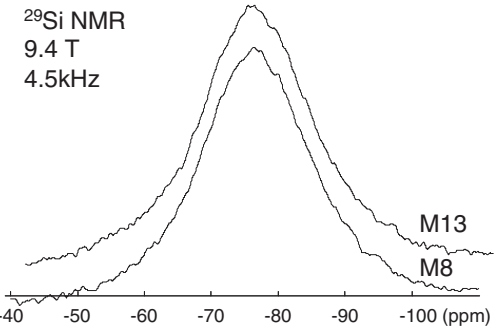

Fig. 2. NMR spectra of the M8 and M13 slags.

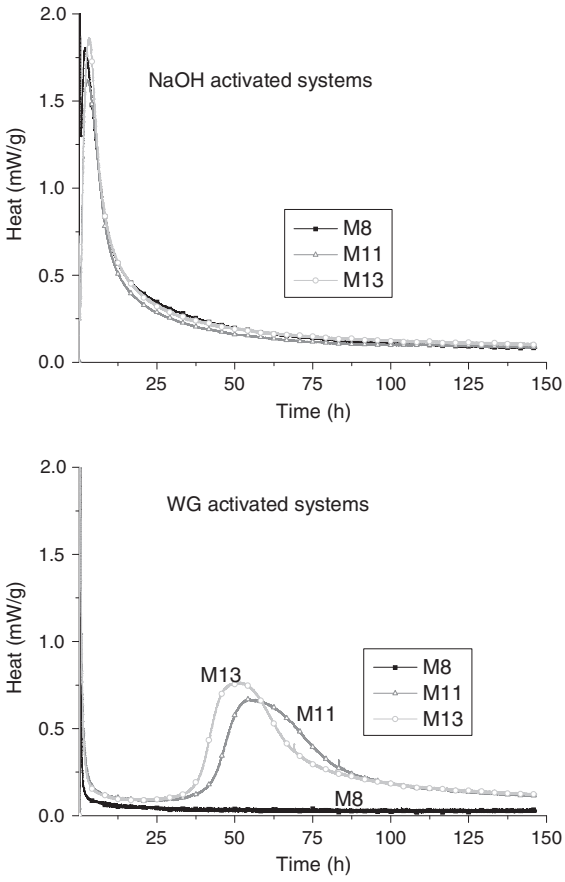

Fig. 3. Influence of the MgO content of the slag on the hydration kinetics.

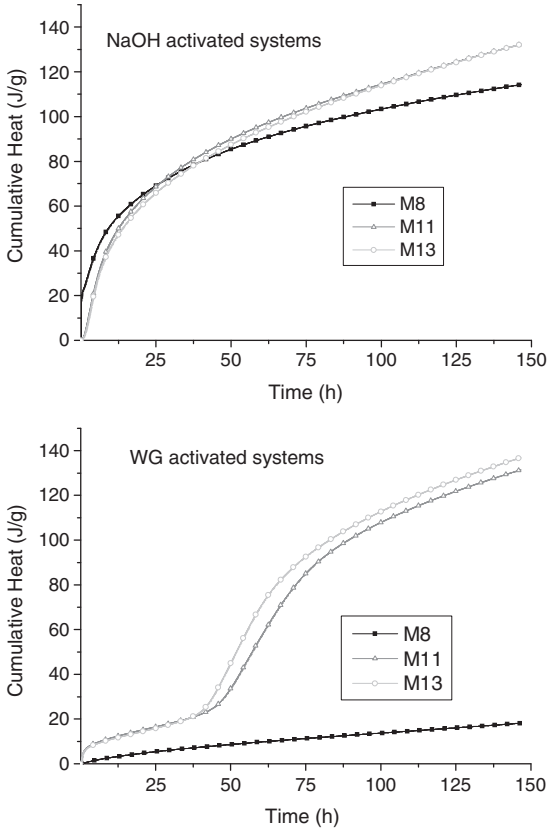

Fig. 4. Influence of the MgO content of the slag on the cumulative heat during hydration.

different hydration times using image analysis (IA) [15–17]. Over 80 images were taken on a large polished section of 20 mm diameter per sample at a magnification of 2500. The minimum pore radius measured corresponds to 0.05 μm. Energy dispersive X-ray spectroscopy (EDX) was applied to determine the elemental compositions of the hydrate assemblage. The analyses were carried out using an accelerating voltage of 15 kV to ensure a good compromise between spatial resolution and adequate excitation of the FeK_α peak. Over 60 points (EDX spots) per sample at each studied age were analysed (see Fig. 7).

2.3.3. Thermodynamic modelling

Thermodynamic calculations were carried out using a consistent set of thermodynamic data [3,18,19], which had been originally compiled and verified for Portland cement systems. A geochemical modelling programme, GEMS [20], was used to calculate the kind and amount of solids precipitated. Based on the molar volume [cm^3/mol] of the phases [18,19] present in the sample, the volume of each individual hydrate as well as the total volume of the hydrating slag was calculated. The measured composition of the slag (XRF data, cf. Table **1**) and the activator was used as input. The uptake of alkalis by C–S–H was approached by using an ideal solid solution model between jennite, tobermorite, $[(KOH)_{2.5}\cdot SiO_2\cdot H_2O]_{0.2}$ and $[(NaOH)_{2.5}\cdot SiO_2\cdot H_2O]_{0.2}$ as proposed by Kulik et al.[21]. The aluminium uptake in the C(−A)–S–H was taken into account based on the EDX measurement. It was assumed that the incorporation of aluminium, which occurs mainly at bridging sites [22,23], does not influence the molar volume of the tobermorite-like C–S–H, as the incorporation of Al has been reported to stabilise the 14-Å tobermorite [24].

3. Analysis of the unhydrated slags

The difference in MgO content may cause differences in the chemical and physical characteristics of the unhydrated slags. Thus a detailed analysis is performed, and the results of the different studied slags are compared.

3.1. Chemical composition

The chemical compositions determined by X-ray fluorescence (XRF) and the granular properties of the three slags are given in Table 1. A small amount of additional metallic iron was observed which originates from the laboratory ball mill.

3.2. XRD

The results of the quantitative phase analysis of the three studied slags are given in Table 2. The different slags exhibit high amorphous contents (>98.5%) and only very minor contents of crystalline phases (melilite and merwinite) (Table 2; Fig. 1).

3.3. ^{29}Si NMR

^{29}Si NMR has been performed to observe the effect of MgO content on the structure of the glassy phase. The method allows distinguishing different chemical neighbourhoods (i.e. coordination) for the nucleus under investigation (in this case ^{29}Si) and to quantify its occurrence in the different coordination states. As Mg^{2+} is a small and highly charged cation, it tends to act as a network modifier and might induce modification of the glass structure with the amount of Mg^{2+}.

The obtained spectra present a broad peak between −40 and −100 ppm (Fig. 2) covering the ^{29}Si chemical shift ranges of Q^0 to Q^3 units. The strong overlapping does not permit any deconvolution of

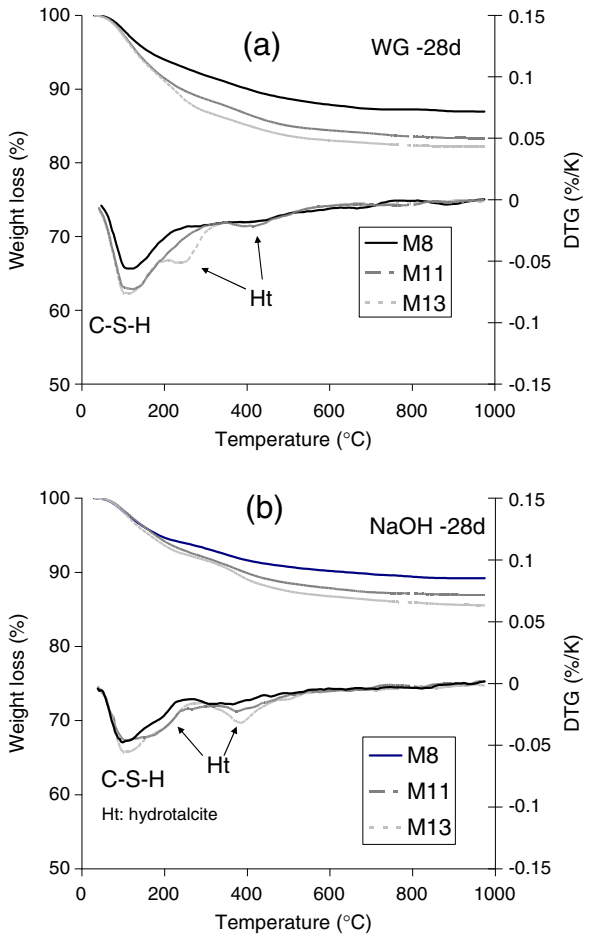

Fig. 5. Influence of the MgO content of the slag on TGA and differential TGA (DTG) curves of the slags with (a) WG and (b) NaOH activation after a hydration time of 28 days.

the signal. There is no change of the NMR signal with the increase of Mg^{2+} meaning that the silicate network composed of Q^0 to Q^3 species is not strongly affected by the amount of Mg^{2+} in the structure. No significant depolymerisation of the silicate network is observed.

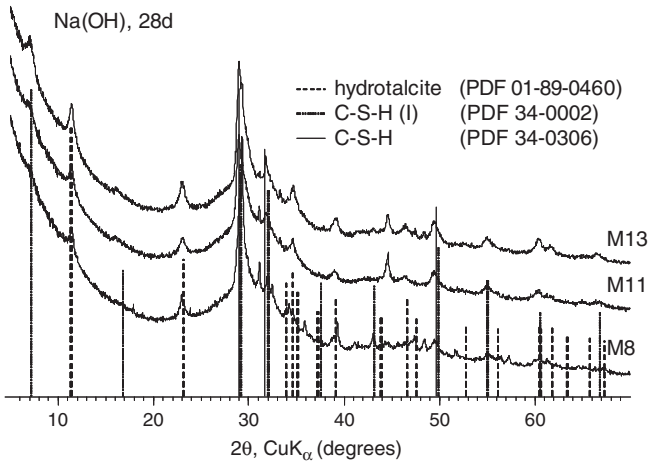

Fig. 6. Comparison of the XRD patterns of the different MgO content NaOH activated slag at 28 days.

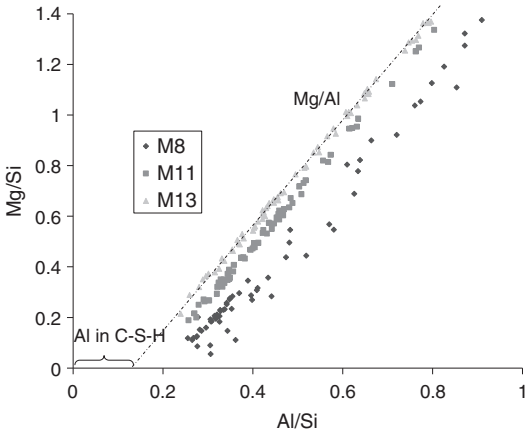

Fig. 7. Influence of the atomic ratios Mg/Si vs. Al/Si of the different slags activated with NaOH at 28 d.

4. Hydration

4.1. Compressive strength

The use of NaOH activator results in a 1 day compressive strength of the pastes of about 8–10 MPa higher than for the WG activated slag (Table 3). After 7 days of hydration, NaOH activated samples show only a moderate strength gain reaching values between 25 and 28 MPa after 1 year. The WG activated slags perform poorly after 1 day, but reveal high compressive strengths between 69 and 105 MPa after 1 year of hydration. These observations agree with other studies [25–30].

With increasing MgO content of the slags a more rapid strength development is obtained for both activators and a higher compressive strength is reached both at early (days) and late (1 year) hydration times. Significantly higher compressive strength is observed for the M11 and M13 compared to the M8 slags, whilst almost no differences between M11 and M13 are observed especially at later ages. The impact of MgO content of the slag is much more pronounced for WG than for NaOH activated slags.

Complementary strength testing was performed on standard mortar prisms. The results show a slight increase with the MgO increase for the WG activated slag but less distinct than observed for the pastes (Table 4).

4.2. Hydration kinetics

4.2.1. Heat of hydration

The comparison of heat evolution and cumulative heat between the different slags using NaOH and water glass as activators is shown in Fig. 3 and Fig. 4. The reaction of slag activated using NaOH is characterised by one main peak after 3 h, which is not significantly influenced by the MgO content of the slag (Fig. 3). Only M8 exhibits a considerable heat development during the first hours but shows a lower cumulative heat after more than 1 day and longer (Fig. 4).

The hydration of the slags activated using WG is characterised by a first peak after 2–4 h and a large second peak corresponding to the

Table 2
Phase composition of the slags by XRD (Rietveld analysis).

	M8	M11	M13
amorphous	99.8%	98.9%	98.5%
melilite	0.2%	0.7%	0.2%
merwinite	n.d	0.5%	1.3%

n. d.: not detectable.

Table 3
Compressive strengths of the slag pastes in MPa (± 2).

	M8		M11		M13	
age (days)	NaOH	WG	NaOH	WG	NaOH	WG
1	8.3	n.m.	9.3	3.1	9.5	3.3
7	13.9	21.5	17.8	32.4	17.3	40.4
28	24.2	44.4	25.4	70.9	27.2	78.7
180	24.9	65.1	28.1	93.9	29.9	108.3
360	25.3	69.1	27.1	94.7	28.4	104.7

n.m.: not measured.

Table 5
Degree of hydration measured by SEM-IA (weight percent ±3%).

	M8		M11		M13	
age (days)	NaOH	WG	NaOH	WG	NaOH	WG
1	30	n.m.	31	n.m.	31	n.m.
7	33	13	37	27	36	32
28	38	38	39	39	39	42
180	44	46	47	46	46	48
360	54	53	56	58	58	57

n.m.: not measured.

main reaction after 2 days of activation in the case of M13 and M11 slags and after more than 6 days for M8. The second exothermal peak is earlier, narrower and more intense for M13 than for M11. The cumulative heat is significantly higher for the M13 and M11 than for M8 up to 6 days. After 6 days the total heat released is highest for the slag with the highest MgO content.

With increasing MgO content of the slags the hydration kinetics during early ages increases. This effect is much more significant between M8 and M11 than between M11 and M13.

4.2.2. Slag dissolution

SEM image analysis gives a reliable estimate of the real degree of reaction of the slag [15,25,31]. The comparison of the quantity of anhydrous slag after different hydration times with the original slag content allows calculating the fraction of slag reacted. An increase of MgO content of the slag increases the hydration degrees (Table 5), which is consistent with calorimetry data (Fig. 3 and Fig. 4) and the strength development (Table 3).

For the slags activated by WG, the initial reaction rate is slow, especially at low MgO content. Only 13% of the M8 slag is reacted after 7 days compared 27 and 32% of the M11 and M13 (Table 5). This is consistent with the calorimetric data, where within the first 6 days no second hydration peak is observed for M8. After 28 days and longer, the observed reaction degrees are more comparable although the high MgO content slags generally showed slightly more slag reaction than M8.

For the NaOH activated slags the initial reaction is much faster and thus the differences in the degree of hydration are smaller, even at 1 and 7 days. However, in all cases a slightly higher degree of reaction of the slags containing more MgO was observed.

At 28 days and longer, a similar degree of reaction is observed for the NaOH and the WG activated slags, consistent with previous observations [25].

4.2.3. Bound water

The bound water content obtained by measuring the weight loss up to 650 °C using TGA can be used as a measure of the hydration kinetics of a slag [32,33]. The comparison between different slags or different activators, however, is problematic as different hydrates with differing water contents also influence the bound water content [25,32]. According to the weight losses given in Table 6, the WG activates the slag much more slowly than the NaOH activator. After longer hydration times, however, the water loss is always higher in the case of WG activator, due to higher binding of water in C–S–H occurring in the WG activated samples (see [25]), whilst the degree of hydration is similar for both activators after 28 days and longer (see above).

The water loss after 1 and 7 days is for M8 considerably lower than for M11 and M13. The differences get smaller with increasing hydration time, and after 28 days bound water contents are similar. However, even after 1 year slightly more water is bound in the slags containing more MgO. This is consistent with the slightly higher degree of slag reaction described above. In addition, the higher amount of hydrotalcite-like phase present (see below), increases the bound water content of the high MgO slags as the hydrotalcite-like phase ($Mg_4Al_2O_7 \cdot 10H_2O$) contains relatively more water than C–S–H.

The general hydration trends of the water loss agree with the degree of reaction determined by SEM-IA. However, as discussed previously [25], not only the degree of reaction determines the water loss but also the composition of the binder and the kind of activator.

4.3. Hydrates

4.3.1. Solid phases

The TGA data as given in Fig. 5 indicate the presence of C–S–H (main weight loss 50–200 °C) and of a hydrotalcite-like solid (weight loss at around 200 °C and 400 °C) [33–35]. Both, C–S–H and hydrotalcite are generally observed in hydrated alkali activated slags [3,5,8,25,36,37]. As discussed above, after long hydration times a lower weight loss is observed for the NaOH activated slags compared to the WG activated slags. In a previous study [25] we found that during the fast early reaction of the NaOH activated slags a dense C–S–H forms, which contains less water compared to the C–S–H in WG activated slags.

XRD reveals the presence of tobermorite like C–S–H phase and of a hydrotalcite-like phase for the WG activated slag. No strätlingite or any other crystalline hydrate could be identified. The hydration pattern becomes more complex for NaOH activated pastes as in addition to the hydrotalcite-like phase and the C–S–H also a more crystalline, sodium rich C(−N)–S–H (labelled as C–S–H (I) in Fig. 6) with a similar Ca/Si is observed, as already previously reported [25]. The C–S–H gels present in NaOH activated pastes are more crystalline and contain less water [25].

The Ca/Si ratio of the C–S–H as given in Table 7 is influenced neither by hydration time nor by the presence of additional MgO. For NaOH activation, Ca/Si is around 0.9, in agreement with the initial

Table 4
Compressive strengths of the mortars samples in MPa (± 2).

	M8		M11		M13	
age (days)	NaOH	WG	NaOH	WG	NaOH	WG
1	6	n.m.	5.8	n.m	5.8	n.m
2	8.3	n.m.	7.3	n.m	7.5	n.m
7	13.9	21.5	11.8	30.4	12.1	30.4
28	18.2	41.4	17.0	42.9	17.4	50.7

n.m.: not measured.

Table 6
Weight loss between 30 °C and 650 °C determined by TGA of the hydrated samples (weight percent relative to the hydrated slag).

	M8		M11		M13	
age (days)	NaOH	WG	NaOH	WG	NaOH	WG
1	9.1	2.4	11.2	9.0	12.5	9.0
7	10.9	2.4	11.9	12.7	12.7	13.8
28	11.4	12.4	13.5	15.7	14.5	17.8
180	12.9	15.6	15.9	17.8	17.5	18.7
360	16.9	19.2	19.2	20.1	19.9	21.7

Table 7
Atomic ratio obtained by EDX analyses (±0.05).

Slag		NaOH			WG		
	age (days)	Ca/Si	Al/Si	Mg/Al	Ca/Si	Al/Si	Mg/Al
M8	1	0.89	0.23	2.15	n.m.	n.m.	n.m.
	7	0.90	0.23	2.12	0.79	0.22	2.09
	28	0.87	0.23	2.14	0.82	0.22	2.05
	180	0.88	0.21	2.10	0.80	0.23	2.04
	360	0.88	0.23	2.09	0.81	0.22	2.01
M11	1	0.91	0.18	2.14	0.82	0.17	2.09
	7	0.88	0.18	2.11	0.83	0.17	2.05
	28	0.87	0.17	2.04	0.81	0.16	2.07
	180	0.89	0.17	2.02	0.82	0.16	2.02
	360	0.92	0.18	2.10	0.77	0.17	2.01
M13	1	0.91	0.15	2.09	0.78	0.16	2.10
	7	0.91	0.15	2.07	0.81	0.14	2.07
	28	0.89	0.15	2.08	0.80	0.14	2.05
	180	0.87	0.15	2.06	0.81	0.15	2.04
	360	0.89	0.15	2.02	0.80	0.14	2.05

n.m.: not measured.

Ca/Si molar ratio of the unhydrated slag of 1.0 (see in Table 1). For WG activation a slightly lower Ca/Si of around 0.8 is observed, caused by the additional SiO_2 from the WG activator ($Na_2SiO_3 \cdot 5H_2O$).

The presence of a positive abscissa in the Mg/Si versus Al/Si ratios in Fig. 7 indicates the presence of Al in the C-S-H and the formation of a hydrotalcite-like phase with an Mg/Al ratio of ~2.1 (Table 7). The Al incorporation in C–S–H does not depend on the sample age or on the type of activator. However, the Al incorporation in C–S–H decreases with increasing MgO content from Al/Si = 0.23 for M8 to 0.17 for M11 and 0.15 for M13, as shown in Table 7. Even at high MgO contents, no magnesium substitution in place of Ca in the C–S–H was observed by EDX analysis.

The shoulders in TGA at 200 and 400 °C associated with the hydrotalcite-like phase are more distinct with higher MgO content (Fig. 5) Also the XRD data indicate that the amount of hydrotalcite increases with the MgO content (Fig. 6). The Mg/Al molar ratio derived from EDX figure (Fig. 7) is constant at a value of 2.0 to 2.1 independent of the activator, MgO content or hydration time (Table 7). This indicates that in all cases hydrotalcite-like phases with a similar composition are formed. This Mg/Al ratio is well within the range reported for hydrotalcite-like phases (1.92 to 4.35) observed in hydrated slag pastes [38,39].

4.3.2. Microstructure

During the first day of hydration, hydrates precipitate around the slag particles in the case of NaOH activator (Fig. 8), whilst none or very little hydrates could be observed for the WG activated samples. In the matrix of high MgO content slags hydrotalcite platelets can be observed at early ages (see Fig. 8).

After 28 days and longer the reacting slag grains of all the studied slags activated by NaOH are surrounded by C–S–H rims (Fig. 9 and Fig. 10). In the case of the WG, no clear rims are found. The C–S–H developed early in the NaOH activated slags exhibits a brighter grey level than the C–S–H in the WG activated systems (Fig. 10) due to the higher density and low water content of the hydrates as reported in a previous study [25]. The samples activated using NaOH have a denser C–S–H, and more pores are visible in the matrix at later ages (Fig. 9 and Fig. 10). Even after one year, a coarser microstructure is observed for the NaOH activated slags, and the hydration products are less homogeneously distributed than in the matrix of the WG activated samples.

The influence of MgO content on the hydration kinetics is also visible in the microstructure. The high MgO content slags have less porosity and less anhydrous slag particles than the low MgO slags up to 28 days (see Fig. 9, Table 5), at later ages the differences become smaller. With higher MgO content less small slag particles are present and the matrix is well developed.

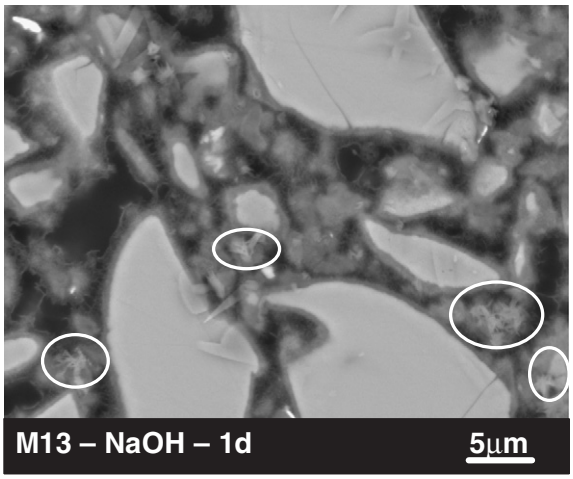

Fig. 8. SEM micrograph of NaOH activated M13 slag after 1 day showing the presence of hydrotalcite platelets (see circles).

The slags activated with NaOH show a coarse porosity around 18 vol.-% after one day, which decreases to a value of about 12 vol.-% after one year (Table 8). No influence of the slag composition is observed. In the case of slags activated with water glass, the porosity after 1 day could not be measured as the samples were not hardened enough to prepare polished sections. After 7 days the porosity decreases with increasing MgO content in accordance with the faster hydration of the M11 and M13 samples. After 28 days and beyond, porosity of the WG activated pastes is very low (max. 3 vol.-%) for all MgO contents.

4.4. Thermodynamic modelling

The thermodynamic calculations indicate that the amount of hydrotalcite-like phase increases with the increasing MgO content as shown in Fig. 11 so that at high MgO content a higher fraction of the available aluminium is bound by the hydrotalcite-like phase ($Mg_4Al_2O_7(H_2O)_{10}$). The remaining aluminium is incorporated in C–S–H. The Al uptake by C–S–H is observed to decrease with increasing MgO content (see Table 7), which is considered in the calculations according to the EDX measurements. At high MgO content, the formation of traces of brucite is predicted, which has not been observed in any of our slags experimentally. This difference could be due to overestimating the Al uptake in C–S–H or due to the slightly higher Mg/Al ratio of approx. 2.1 in the experimentally observed hydrotalcite-like phase, whilst in the calculations a slightly lower Mg/Al of 2.0 was used due to absence of solubility products of hydrotalcite containing more MgO, e.g. $Mg_6Al_2O_9(H_2O)_{12}$ in the thermodynamic database used [18,19]. From the literature it is known that a large range of hydrotalcite compositions is stable, from 1.95 to 4.95 [4,35,40]. At very low MgO contents (<7%), the formation of strätlingite is predicted. At higher MgO contents more hydrotalcite-like phase is calculated to form and less C–S–H. Due to the lower density of the hydrotalcite-like phase (2.0 g/cm^3) [19,41] compared to the density of 2.23 g/cm^3 of a tobermorite like C–S–H ($(CaO)_{0.83}\ SiO_2 \cdot (H_2O)_{1.3}$, [42]), a higher hydrate volume is predicted and thus a lower porosity. Calculations indicate a 9% higher volume of the hydrates for M13 compared to M8 (Fig. 11). The effect is increased as at higher MgO contents less Al is incorporated in the C–S–H but forms hydrotalcite.

Generally the predicted phase assemblage is in all systems in good agreement with the experimental results where C–S–H as well as hydrotalcite-like phases have been found. For all investigated slags the same hydrate assemblage was calculated. The main difference calculated was the formation of a C–S–H with a lower Ca/Si ratio in the presence of WG and 5% more C–S–H when compared to NaOH

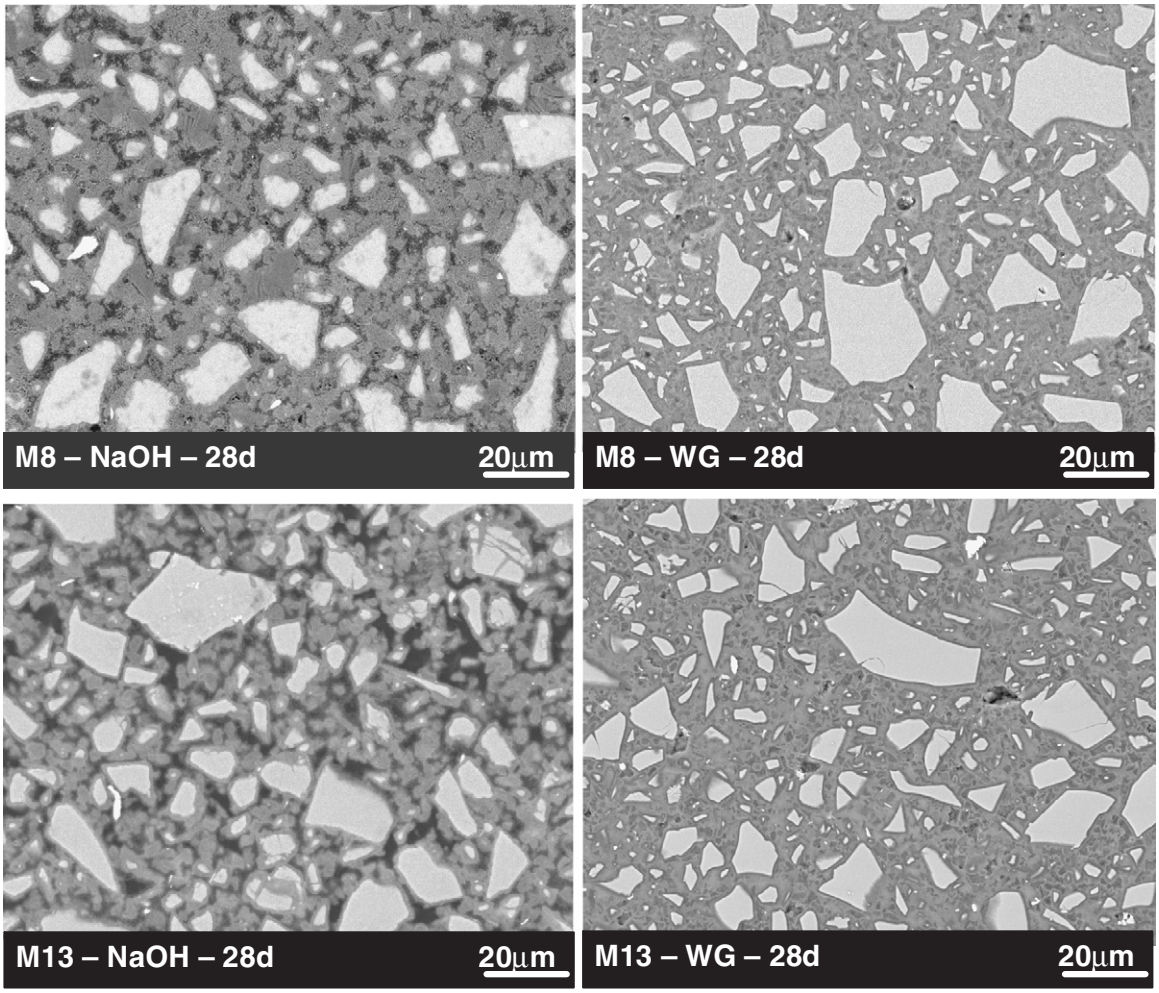

Fig. 9. Microstructure of alkali activated slags M8 and M13 after 28 days of hydration.

activated systems. The calculated Ca/Si ratio in the slag C–S–H is 1.05 for the NaOH activated slags and 0.94 for the system activated with water glass (due to the introduction of SiO_2 with the activator) regardless of the MgO content. The trends agree well with experimental observations in which we observed the same hydration products but a lower Ca/Si ratio in WG-activated slags. The alkaline activator type influences mainly the rate of hydration and the amount of water in the C–S–H, but the same kind of hydrates is formed.

5. Discussions and conclusions

For all slags investigated, the activation by NaOH led to a faster initial reaction and higher early compressive strength than observed for the water glass activated slags. At later ages, however, a similar degree of reaction is observed for both activators. Dense hydrate rims are formed during the fast early reaction of the NaOH activated slags resulting in a larger coarse porosity and a lower compressive strength at later ages compared with WG activated samples, although comparable degrees of slag reaction are observed (Fig. 12), as already discussed in detail in a previous paper [25].

The changes in the MgO content of a blast furnace slag influence the kinetics of the alkali activated systems and change the amount of hydrates formed:

i) The samples with the lowest MgO content activated with WG show a very low hydration heat flow at early ages. This is consistent with the lower compressive strengths and the slow reaction of the slag observed. The slags containing more MgO show higher cumulative heat up to 6 days, a higher degree of reaction and more strength up to 7 days. The NaOH activated slags show faster kinetics and less differences between the different MgO contents, but at later ages a much lower compressive strength compared to the WG activated slags.

ii) Experimental observations as well as thermodynamic modelling predict the same phase assemblage with the main hydration products C–S–H and hydrotalcite-like phase, in the case of the low MgO slag also possibly traces of strätlingite. Higher MgO content in the slag increased the quantity of hydrotalcite-like phase in the hydrate assemblage and decreased the Al uptake by the C–S–H.

iii) The MgO content of the slag is found to influence at longer hydration times mainly the amount of the hydrotalcite-like phase formed. At higher MgO contents more voluminous hydrotalcite is calculated to precipitate and less C–S–H and thus a higher volume of the hydrates and a lower porosity (Fig. 11).

- In the NaOH activated system, the higher MgO content leads to a slightly higher degree of reaction and thus to a slightly higher (approx. 3 MPa) compressive strength at all ages. The increase of the amount of hydrotalcite-like phase and thus the higher calculated volume (+9%, Fig. 11) at higher MgO contents has no significant effect on the compressive strength of the NaOH activated slags as

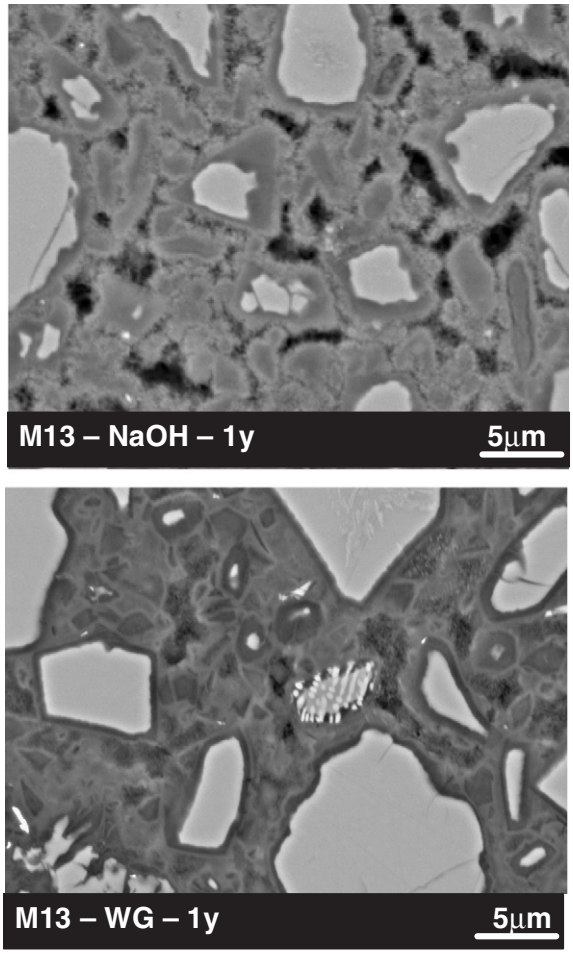

Fig. 10. SEM-micrograph of NaOH and WG activated slag containing 13% of MgO after 1 year.

shown in Fig. 12a. Also the measured coarse porosity is not decreased in the presence of more hydrotalcite-like phase.

- In the case of WG activated slags, the high MgO slags show a much higher compressive strength than the slag M8 at the same degree of hydration (Fig. 12a). The compressive strengths are clearly related to the coarse porosity and no differences between the different MgO contents are observed (Fig. 12b). This indicates that the 9% higher volumes of hydrates formed for M13 compared to M8 and the resulting lower porosity is responsible for the 50 to 80% increase of the compressive strength in the paste samples after 28 days and longer. In the mortar prisms, the increase was lower probably due to the reduction of the pastes volume to 40% of the total volume of the mortar samples.

Table 8
Coarse capillary porosity measured by SEM-IA (volume percent ± 1%).

	M8		M11		M13	
age (days)	NaOH	WG	NaOH	WG	NaOH	WG
1	17.5	n.m.	17.5	n.m.	16.9	n.m.
7	15.3	17.7	14.3	5.9	14.1	2.2
28	13.2	2.8	12.6	1.0	11.5	0.6
180	12.7	2.6	12.5	0.9	12.2	0.5
360	12.6	2.6	12.5	0.8	12.1	0.4

n.m.: not measured.

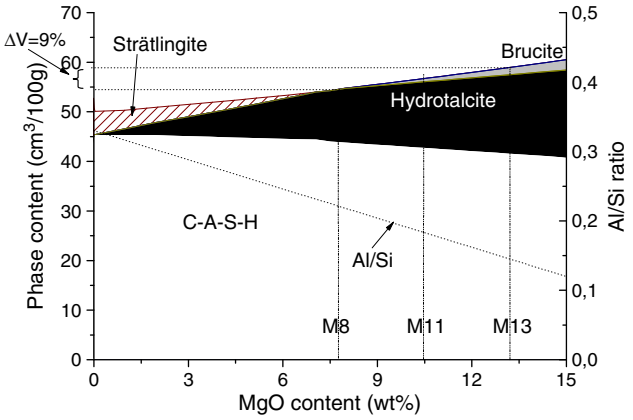

Fig. 11. Influence of MgO content on the hydrates present in NaOH activated slag. The Al content in the C–S–H was varied (Al/Si = 0.33–0.014 MgO (wt%)) based on the Al uptake observed by EDX.

- What causes the strongly different behaviour of the NaOH activated slag is not clear. Possibly the fast early reaction in these systems and the formation of the dense hydrate layer at early ages masks the higher volume of the hydrates of the high MgO slags.

The increase of hydrate volume and the corresponding higher compressive strength with higher MgO content is relevant for alkali activated slags only. In supersulfated slags or in Portland cement–slag

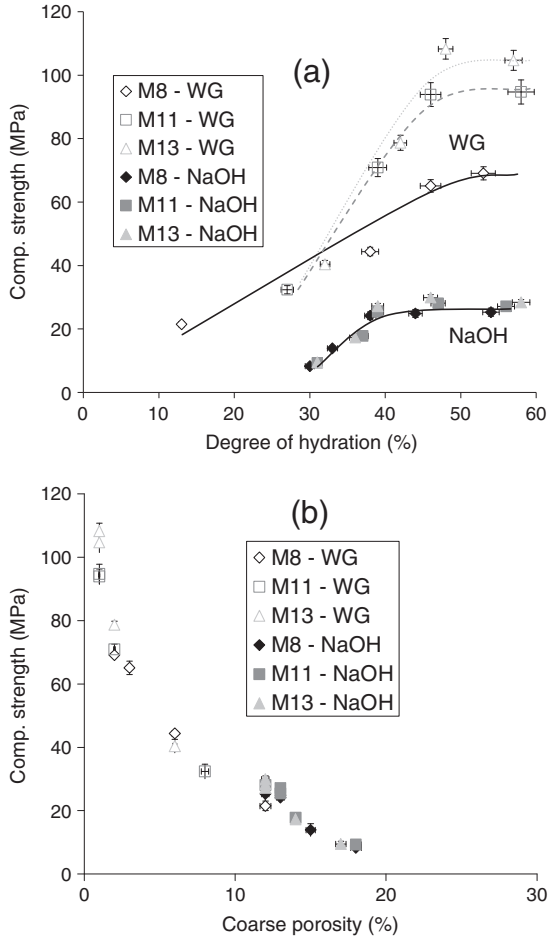

Fig. 12. Compressive strength of the pastes vs. (a) degree of hydration and (b) coarse porosity of the different slags. The lines are intended as eye guides only.

blends, other hydrates are formed and the presence of additional MgO might decrease compressive strength as reported for Portland cement–slag blended mortars [11].

Acknowledgements

The authors would like to acknowledge Walter Trindler and Boris Ingold for their help with the experimental work.

References

[1] E. Gartner, Industrially interesting approaches to "low-CO_2" cements, Cement and Concrete Research 34 (2004) 1489–1498.
[2] M.C.G. Juenger, F. Winnefeld, J.L. Provis, J.H. Ideker, Advances in alternative cementitious binders, Cement and Concrete Research, In press.
[3] B. Lothenbach, A. Gruskovnjak, Hydration of alkali-activated slag: thermodynamic modelling, Advances in cement research 19 (2007) 81–92.
[4] I.G. Richardson, A.R. Brough, G.W. Groves, C.M. Dobson, The characterization of hardened alkali-activated blast-furnace slag pastes and the nature of the calcium silicate hydrate (C-S-H) phase, Cement and Concrete Research 24 (1994) 813–829.
[5] S.-D. Wang, K.L. Scrivener, Hydration products of alkali activated slag cement, Cement and Concrete Research 25 (1995) 561–571.
[6] S. Caijun, L. Yinyu, Investigation on some factors affecting the characteristics of alkali-phosphorus slag cement, Cement and Concrete Research 19 (1989) 527–533.
[7] A. Gruskovnjak, B. Lothenbach, F. Winnefeld, R. Figi, S.C. Ko, M. Adler, U. Mäder, Hydration mechanisms of super sulphated slag cement, Cement and Concrete Research 38 (2008) 983–992.
[8] H.F.W. Taylor, Cement Chemistry, in: A.S.o.C. Engineers (Ed.), Second Edition, 1997, p. 480.
[9] H.P. Sun, K. Nakashima, K. Mori, Influence of slag composition on slag–iron interfacial tension, Isij International 46 (2006) 407–412.
[10] L. Shousun, Effect of MgO in steel slag on soundness of cement, 7th International Conference on Cement Chemistry, Paris, 1980, pp. III–25.
[11] W. Wassing, Relationship between the chemical reactivity of granulated blastfurnace slags and the mortar standard compressive strength of the blastfurnace cements produced from them, Cement International 1 (2003) 95–109.
[12] E. Demoulian, P. Gourdin, F. Hawthorn, C. Vernet, Influence of slags chemical composition and texture on their hydraulicity, 7th International Conference on Cement Chemistry, Paris, 1980, pp. III–89.
[13] G. Le Saout, T. Füllmann, V. Kocaba, K. Scrivener, Quantitative study of cementitous materials by X-ray diffraction/Rietveld analysis using an external standard, 12th International Congress on the Chemistry of Cement Montréal, Canada, 2007.
[14] G. Le Saoût, V. Kocaba, K. Scrivener, Application of the Rietveld method to the analysis of anhydrous cement, Cement and Concrete Research, 41 133–148.
[15] M. Ben Haha, K. De Weerdt, B. Lothenbach, Quantification of the degree of reaction of fly ash, Cement and Concrete Research 40 (2010) 1620–1629.
[16] K.L. Scrivener, Backscattered electron imaging of cementitious microstructures: understanding and quantification, Cement and Concrete Composites 26 (2004) 935–945.
[17] K.L. Scrivener, H.H. Patel, P.L. Pratt, L.J. Parrott, Analysis of phases in cement paste using backscattered electron images, methanol adsorption and thermogravimetric analysis, Proceeding Material Research Society Symposium, Microstructural Development During the Hydration of Cement, 1986 67–76.
[18] T. Matschei, B. Lothenbach, F.P. Glasser, Thermodynamic properties of Portland cement hydrates in the system $CaO–Al_2O_3–SiO_2–CaSO_4–CaCO_3–H_2O$, Cement and Concrete Research 37 (2007) 1379–1410.
[19] B. Lothenbach, T. Matschei, G. Möschner, F.P. Glasser, Thermodynamic modelling of the effect of temperature on the hydration and porosity of Portland cement, Cement and Concrete Research 38 (2008) 1–18.
[20] D. Kulik, U. Berner, E. Curti, Modelling chemical equilibrium partitioning with the GEMS-PSI code, in: B. Smith, B. Gschwend (Eds.), Nuclear Energy and Safety, PSI Scientific Report 2003, Paul Scherrer Institute, Villigen, Switzerland, 2004, pp. 109–122.
[21] D. Kulik, J. Tits, E. Wieland, Aqueous–solid solution model of strontium uptake in C–S–H phases, Geochimica et Cosmochimica Acta 71 (2007) A530.
[22] P. Yu, R.J. Kirkpatrick, B. Poe, P.F. McMillan, X. Cong, Structure of calcium silicate hydrate (C–S–H): near-mid-, and far-infrared spectroscopy, Journal of the American Ceramic Society 82 (1999) 742–748.
[23] I.G. Richardson, G.W. Groves, The incorporation of minor and trace elements into calcium silicate hydrates (C–S–H) gel in hardened cement pastes, Cement and Concrete Research 23 (1993) 131–138.
[24] G. Renaudin, J. Russias, F. Leroux, F. Frizon, C. Cau-dit-Coumes, Structural characterization of C–S–H and C–A–S–H samples -Part I: long-range order investigated by Rietveld analyses, Journal of Solid State Chemistry 182 (2009) 3312–3319.
[25] M. Ben Haha, G. Le Saout, F. Winnefeld, B. Lothenbach, Influence of activator type on hydration kinetics, hydrate assemblage and microstructural development of alkali activated blast-furnace slags, Cement and Concrete Research 41 (2011) 301–310.
[26] A.R. Brough, A. Atkinson, Sodium silicate-based, alkali-activated slag mortars: Part I. Strength, hydration and microstructure, Cement and Concrete Research 32 (2002) 865–879.
[27] J.I. Escalante-García, J.H. Sharp, The microstructure and mechanical properties of blended cements hydrated at various temperatures, Cement and Concrete Research 31 (2001) 695–702.
[28] A. Fernández-Jiménez, J.G. Palomo, F. Puertas, Alkali-activated slag mortars: mechanical strength behaviour, Cement and Concrete Research 29 (1999) 1313–1321.
[29] A. Fernandez-Jimenez, F. Puertas, Effect of activator mix on the hydration and strength behaviour of alkali-activated slag cements, Advances in Cement Research 15 (2003) 129–136.
[30] D.M. Roy, Alkali-activated cements opportunities and challenges, Cement and Concrete Research 29 (1999) 249–254.
[31] M. Ben Haha, E. Gallucci, A. Guidoum, K.L. Scrivener, Relation of expansion due to alkali silica reaction to the degree of reaction measured by SEM image analysis, Cement and Concrete Research 37 (2007) 1206–1214.
[32] J.I. Escalante-Garcia, A.F. Fuentes, A. Gorokhovsky, P.E. Fraire-Luna, G. Mendoza-Suarez, Hydration products and reactivity of blast-furnace slag activated by various alkalis, Journal of the American Ceramic Society 86 (2003) 2148–2153.
[33] A. Gruskovnjak, B. Lothenbach, F. Winnefeld, B. Münch, R. Figi, S. Ko, M. Adler, U. Mäder, Quantification of hydration phases in supersulphated cements : review and new approaches, Advances in Cement Research, (accepted).
[34] E. Kanezaki, Thermal behavior of the hydrotalcite-like layered structure of Mg and Al-layered double hydroxides with interlayer carbonate by means of in situ powder HTXRD and DTA/TG, Solid State Ionics 106 (1998) 279–284.
[35] K. Rozov, U. Berner, C. Taviot-Gueho, F. Leroux, G. Renaudin, D. Kulik, L.W. Diamond, Synthesis and characterization of the LDH hydrotalcite–pyroaurite solid-solution series, Cement and Concrete Research 40 (2010) 1248–1254.
[36] A. Gruskovnjak, B. Lothenbach, L. Holzer, R. Figi, F. Winnefeld, Hydration of alkali-activated slag: comparison with ordinary Portland cement, Advances in Cement Research 18 (2006) 119–128.
[37] F. Puertas, A. Fernández-Jiménez, Mineralogical and microstructural characterisation of alkali-activated fly ash/slag pastes, Cement and Concrete Composites 25 (2003) 287–292.
[38] I.G. Richardson, Tobermorite/jennite- and tobermorite/calcium hydroxide-based models for the structure of C–S–H: applicability to hardened pastes of tricalcium silicate, [beta]-dicalcium silicate, Portland cement, and blends of Portland cement with blast-furnace slag, metakaolin, or silica fume, Cement and Concrete Research 34 (2004) 1733–1777.
[39] S.-D. Wang, K.L. Scrivener, ^{29}Si and ^{27}Al NMR study of alkali-activated slag, Cement and Concrete Research 33 (2003) 769–774.
[40] G. Fornasari, R. Glöckler, M. Livi, A. Vaccari, Role of the Mg/Al atomic ratio in hydrotalcite-based catalysts for NOx storage/reduction, Applied Clay Science 29 (2005) 258–266.
[41] G. Mascolo, O. Marino, MgO-bearing phases in the hydration products of slag cement, 7th International Conference on Cement Chemistry, Paris, 1980, pp. III–58.
[42] E. Bonaccorsi, S. Merlino, A.R. Kampf, The crystal structure of tobermorite 14 A (Plombierite), a C–S–H phase, Journal of the American Ceramic Society 88 (2005) 505–512.